Faraday Discussions

Cite this: *Faraday Discuss.*, 2024, **248**, 102

PAPER

Effect of alkali-metal cation on oxygen adsorption at Pt single-crystal electrodes in non-aqueous electrolytes

Julia Fernández-Vidal, †[a] Laurence J. Hardwick, [a] Gema Cabello‡[a] and Gary A. Attard *[b]

Received 26th April 2023, Accepted 24th May 2023
DOI: 10.1039/d3fd00084b

The effect of Group 1 alkali-metal cations (Na^+, K^+, and Cs^+) on the oxygen reduction and evolution reactions (ORR and OER) using dimethyl sulfoxide (DMSO)-based electrolytes was investigated. Cyclic voltammetry (CV) utilising different Pt-electrode surfaces (polycrystalline Pt, Pt(111) and Pt(100)) was undertaken to investigate the influence of surface structure upon the ORR and OER. For K^+ and Cs^+, negligible variation in the CV response (in contrast to Na^+) was observed using Pt(111), Pt(100) and Pt(poly) electrodes, consistent with a weak surface-metal/superoxide complex interaction. Indeed, changes in the half-wave potentials ($E_{1/2}$) and relative intensities of the redox peaks corresponding to superoxy (O_2^-) and peroxy (O_2^{2-}) ion formation were consistent with a solution-mediated mechanism for larger cations, such as Cs^+. Support for this finding was obtained *via in situ* shell-isolated nanoparticle-enhanced Raman spectroscopy (SHINERS). During the ORR and in the presence of Cs^+, O_2^- and weakly adsorbed caesium superoxide (CsO_2) species were detected. Because DMSO was found to strongly interact with the surface at potentials associated with the ORR, CsO_2 was readily displaced at more negative potentials *via* increased solvent adsorption at the surface. This finding highlights the important impact of the solvent during ORR/OER reactions.

Introduction

Lithium–oxygen ($Li–O_2$) batteries have become of particular interest due to their high theoretical specific energy (3505 W h kg^{-1} for the non-aqueous system) compared to the commonly used Li-ion batteries.[1] Studies of $Li–O_2$ systems in

[a]*Stephenson Institute for Renewable Energy, Department of Chemistry, University of Liverpool, Peach Street, L69 7ZF Liverpool, UK*

[b]*Department of Physics, University of Liverpool, Crown Street, L69 7ZD Liverpool, UK. E-mail: attard@liverpool.ac.uk*

† Present address: Leiden Institute of Chemistry, Leiden University, Einsteinweg 55, 2333 CC Leiden, The Netherlands.

‡ Present address: SLB Cambridge Research, High Cross, Madingley Road, CB3 0EL Cambridge, UK.

non-aqueous electrolytes have shown that on Au, Pt, and C surfaces, lithium peroxide (Li_2O_2) is the main product of the oxygen reduction reaction (ORR).[2–5] The precipitation of solid Li_2O_2 during the ORR passivates the electrode surface and blocks the electrode active sites, reducing any catalytic effect of the surface, which leads to the occurrence of parasitic reactions associated with the generation of singlet oxygen.[2,6–8]

In 2013, Hartmann *et al.*[9] and Ren *et al.*[10] demonstrated that the irreversibility presented by the two-electron reduction of O_2 to Li_2O_2 could be improved by the formation of an oxygen/superoxide redox couple that enables a single-electron reversible oxygen reduction reaction/oxygen evolution reaction (ORR/OER) process with high specific energy (w_{th} = 1605 W h kg^{-1} for Na_2O_2)[9] and avoids the formation of solid peroxide species that passivate the electrode surface.

In non-aqueous Li^+-containing electrolytes, control of the product stability and reduced oxygen species[11,12] through electrolyte solvation can be achieved by using solvents with increased Gutmann donor numbers.[13,14] High Gutmann-donor-number solvents allow the formation of Li^+/O_2^- ion pairs that react within the double layer, offering a preferred solution-based mechanism that avoids the passivation of the electrode and enhances the sluggish kinetics of the ORR.[15] The reversible formation of superoxide (O_2^-) and peroxide (O_2^{2-}) species has been detected on charge/discharge as the main products, together with some minor degradation observed over time for Li systems in dimethyl sulfoxide (DMSO).[16,17] DMSO presents a relatively high Gutmann donor number of 29.8 kcal mol^{-1},[18,19] based on the nucleophilic properties of the solvent and high stability.[20]

The size of the cations has been demonstrated to affect the ORR activity.[27–32] In aqueous systems, the cation hydration energy and non-covalent interactions between hydrated alkali-metal cations and OH_{ads} have been highlighted in this regard.[21–23] In Li-containing aprotic electrolytes, the ORR occurs almost exclusively with Li_2O_2 as the reaction product.[3,4] Conversely, as one moves down the Group 1 metals, the reaction mechanism favours the formation of significant amounts of both O_2^{2-} and O_2^- species.[24,25] Indeed, within aprotic electrolytes, the ORR pathway has also been proved to depend on the cation size.[9,10,26] Studies of the Group 1 alkali metals have mostly focused on the smaller cations with investigations being predominantly confined to Li^+ and Na^+.[24,27–31] K–O_2 batteries[32–34] have attracted recent interest due to the reduced overpotential reported in the absence of catalysts and redox mediators compared to Li–O_2 batteries.[10] Nevertheless, despite the ongoing investigations into the ORR, observation of mechanistic details at the interface for different cations remains elusive.[35–37]

Pt has been demonstrated to be one of the most efficient catalysts for the ORR in both aqueous and aprotic electrolytes on model systems.[38–40] In the past decade, *in situ* shell-isolated nanoparticle-enhanced Raman spectroscopy (SHINERS) has proven to be a powerful method to detect surface intermediates.[41,42] Specifically, *in situ* SHINERS studies on Pt single-crystal electrodes have been successfully used to investigate the adsorption of ORR intermediates in aqueous electrolytes[43–45] and also the Na–O_2 non-aqueous system.[4,24] However, despite the success of this approach, there is still a paucity of combined single-crystal/*in situ* SHINERS investigations involving non-aqueous electrolytes to afford a fundamental molecular level insight into the ORR processes associated with metal–oxygen battery systems, probably due to the experimental challenges

that such studies present. Hence, in this work, we perform a qualitative study on the effect that the cation size has on the ORR and OER using such an approach. From SHINERS measurements, the key role that DMSO solvent molecules play in the displacement of adsorbed Cs-cation–superoxide moieties, formed in the initial oxygen reduction step, is demonstrated. Together with cyclic voltammetry (CV) data, showing negligible surface structural sensitivity towards reduction processes involving caesium and oxygen, a strong contrast with the analogous sodium-cation/oxygen redox system is revealed.

Experimental

Chemicals

Dimethyl sulfoxide (DMSO) (>99.9% Hi-Dry®, ROMIL), dried and purified by distillation, was stored inside a glovebox over molecular sieves to ensure an H_2O content <4 ppm. Alkali-metal salts $NaClO_4$ (≥98.0%), $KClO_4$ (≥99.99%), and $CsClO_4$ (≥99.995%), from Sigma-Aldrich, were dried under vacuum at 80 °C overnight and stored inside a glovebox prior to use. Up to N5-purity Ar (≥99.998%, BOC) and O_2 (≥99.999%, BOC) gases, dried by passing through a desiccant (P_2O_5)-filled drying tube, were used for purging and bubbling the electrolytes, respectively, whilst not contaminating the glovebox atmosphere.

Pt single-crystal preparation

Clavilier[46] half-bead Pt(111) and (100) single crystals were annealed with a butane flame and then cooled in a bubbler containing Milli-Q® water and a steady flow of 5% H_2 in Ar to produce a well-ordered surface, and subsequently quenched with a drop of Milli-Q® water (18.2 MΩ cm resistivity). The single crystal was then dipped in 1 mM NaBr (≥99.0%, Sigma-Aldrich) solution, to protect the surface *via* the formation of an irreversibly adsorbed bromine adlayer (Fig. 1).[47] The electrode was then dried under vacuum, transferred to a glovebox, and cycled 5–10 times to achieve a clean electrode surface, free of Br adatoms on the surface.

Polycrystalline Pt preparation

Pt polycrystalline disk electrodes embedded in polyether ether ketone (PEEK) were polished using three different suspensions of decreasing-grain-size alumina (0.1 μm, 0.3 μm and 0.05 μm), then rinsed with ethanol and Milli-Q® water, and finally sonicated in water. The Pt(poly) electrodes were dried at 80 °C overnight under vacuum and then introduced into a glovebox (argon atmosphere; O_2, H_2O <0.1 ppm).

Meniscus configuration

Pt half-bead single crystals were used under a meniscus configuration to ensure that the voltammetric profile corresponded exclusively to the well-oriented face of the electrode. The meniscus configuration avoids voltammetric features originating from the poly-oriented sides of the electrode, as depicted in Fig. 2a. To address the role of the meniscus[48] in O_2 diffusion during the ORR/OER, Pt(poly) electrodes have also been used in the traditional configuration, inserted flat in the electrolyte, as represented in Fig. 2b.

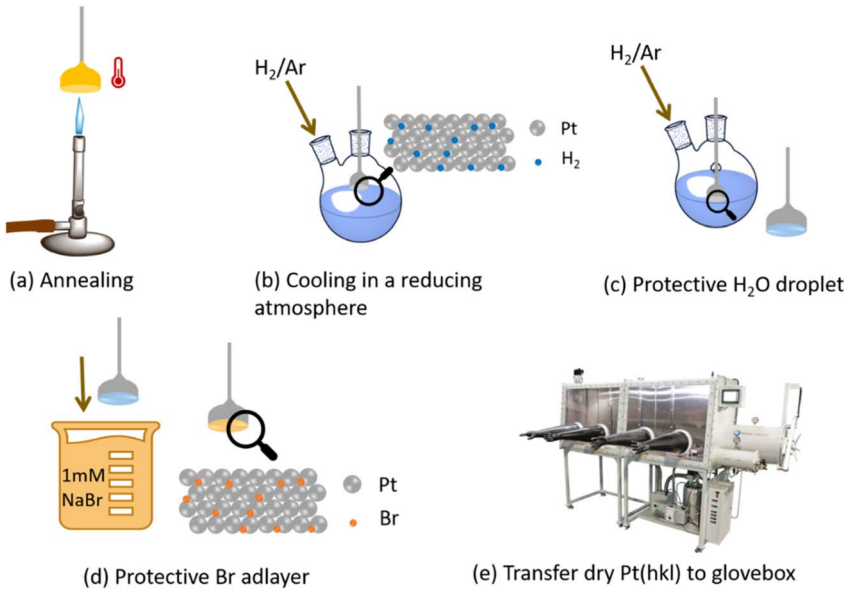

Fig. 1 Schematic description of single-crystal preparation for non-aqueous electrochemical studies. Reproduced from Galloway *et al.*[24] with permission from the Royal Society of Chemistry.

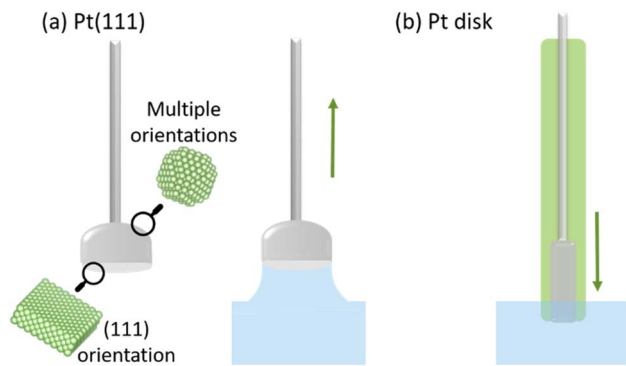

Fig. 2 (a) Schematic of a Pt single-crystal electrode with a (111) facet on the flat side under meniscus configuration. Hard-sphere model made with VESTA software.[49] (b) Schematic of a Pt polycrystalline disk electrode in contact with the electrolyte.

Electrochemistry

Electrochemical experiments were conducted using a BioLogic (VSP-100) potentiostat in an Ar glovebox with moisture levels <1 ppm. Cyclic voltammetry experiments in the present study were carried out in a standard 3-electrode electrochemical cell. A silver wire was used as a pseudo-reference electrode. The Ag/Ag^+ couple was calibrated with the ferrocene/ferrocenium redox couple (E^0_{Fc/Fc^+} = +680 mV *vs.* SHE in DMSO).[50] All potentials are displayed *vs.* the calibrated Ag/Ag^+ redox couple to allow accurate comparison between experiments.

Synthesis of shell-isolated nanoparticles for enhanced Raman spectroscopy

The synthesis of the Au core was carried out using the Turkevich–Frens citrate-reduction method.[51–53] 200 mL of a solution containing 0.01% $HAuCl_4 \cdot nH_2O$ (99.995%, Sigma-Aldrich) were heated under vigorous stirring until boiling. 1.5 mL of a freshly prepared 1% $Na_3C_6H_5O_7 \cdot 2H_2O$ (≥99.5%, Sigma-Aldrich) solution were immediately added to achieve a nanoparticle size of approximately ~55 nm. The protocol developed by Liz-Marzán and co-workers[54,55] and used by Li *et al.*[56] for SHINERS was followed for SiO_2 shell synthesis. Suitability of the silica shells for SHINERS was checked *via* the detection or absence of a Raman-active molecule (pyridine) on Au and Si substrates, respectively.[42]

In situ Raman measurements

Raman measurements were carried out with a Raman spectrometer (Renishaw inVia) with an inverted microscope *via* a 50× objective (Leica), using a 633 nm laser with an exposure time of 10 s and 5 acquisitions. Pt wire was used in the spectro-electrochemical cell as a counter electrode and Ag wire as a reference. Long sealing screw caps were used to both isolate the cell and avoid any contaminants from dissolving into the electrolyte.

Results and discussion

Pt(111) cyclic voltammetry in 0.1 M $NaClO_4$ in DMSO electrolyte is displayed in Fig. 3. All the voltammetric features observed correspond exclusively to the adsorption of oxygen species onto the Pt electrode surface, as can be gleaned by the lack of faradaic current in the Ar-purged electrolyte.

The Na–O_2 system on Pt basal planes has been previously studied in detail and the reaction mechanisms have been identified through *in situ* Raman microscopy.[24] The electrochemical behaviour of different single-crystal facets demonstrated that both O_2^- and O_2^{2-} species are formed during the ORR in the presence of Na^+. In agreement with the literature,[11] for Pt(111) the peak at −0.55 V (I) observed in the reduction sweep in Fig. 3 corresponds to the reduction of O_2 *via* formation of metal–O_2^-, according to:

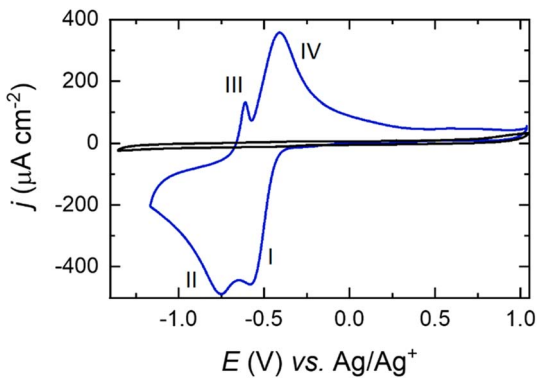

Fig. 3 Cyclic voltammograms of a Pt(111) electrode in a solution containing 0.1 M $NaClO_4$ in DMSO, for Ar- (black) and O_2- (blue) saturated solutions. Scan rate: 50 mV s^{-1} at 23 °C.

$$O_2 + Na^+ + e^- \rightarrow NaO_2 \quad (1)$$

The second reduction peak at around −0.75 V (II) corresponds to a second electron reduction that forms the metal–O_2^{2-}:[57]

$$NaO_2 + Na^+ + e^- \rightarrow Na_2O_2 \quad (2)$$

In the oxidation sweep, two peaks at −0.60 V (III) and −0.40 V (IV) are observed, which constitute the OER:

$$Na_2O_2 \rightarrow NaO_2 + Na^+ + e^- \quad (3)$$

$$NaO_2 \rightarrow O_2 + Na^+ + e^- \quad (4)$$

As with Na^+, for K^+ and Cs^+, the ORR proceeds *via* two quasi-reversible electrochemical processes with two main reduction steps involving the formation of O_2^- and O_2^{2-} species (Fig. 4).[57–61]

The half-wave potential ($E_{1/2}$) corresponding to the ion-pair formation between the alkali metal and O_2^- shifts towards more negative potentials for smaller cations ($Na^+ > K^+ > Cs^+$ – Table 1), while the $E_{1/2}$ corresponding to the formation of O_2^{2-} follows the opposite trend (Table 2).

With a Na^+-containing electrolyte, Galloway *et al.*[24] studied the adsorption of species using different Pt(*hkl*) surfaces and demonstrated the surface specificity

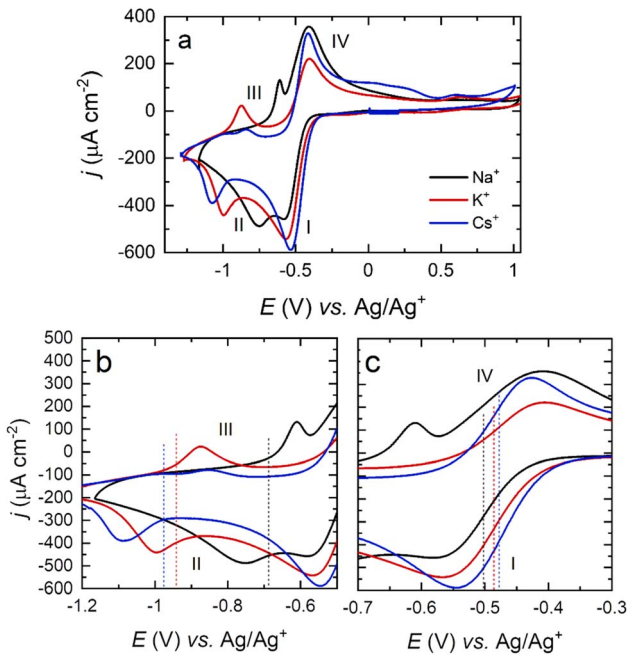

Fig. 4 (a) Cyclic voltammograms of a Pt(111) electrode in an O_2-saturated DMSO solution containing 0.1 M $NaClO_4$ (black), $KClO_4$ (red) and $CsClO_4$ (blue). Scan rate: 50 mV s^{-1}. Expanded view of the peaks relating to the formation of O_2^{2-} (b) and O_2^- (c). Dotted lines represent the calculated $E_{1/2}$ of the ORR half reactions for Na^+ (black), K^+ (red) and Cs^+ (blue).

Table 1 Ionic radii of alkali metals Na^+, K^+, and Cs^+. Values taken from the literature[62] are given in Ångström

Group 1 metal ion	Ionic radii (Å)
Na^+	1.02
K^+	1.38
Cs^+	1.67

Table 2 Half-wave peak potential for the formation of superoxide and peroxide species among different alkali cation sizes, for Pt(111) and Pt(poly). Values have been taken from the peak potentials $\left(E_{1/2} = \frac{E_{\text{anodic}} + E_{\text{cathodic}}}{2}\right)$ presented in Fig. 4 for Pt(111) and Fig. 5 for Pt(poly)

	NaO_2	KO_2	CsO_2	Na_2O_2	K_2O_2	Cs_2O_2
Pt(111)	−0.50 V	−0.48 V	−0.47 V	−0.69 V	−0.93 V	−0.97 V
Pt(poly)	−0.53 V	−0.52 V	−0.50 V	−0.71 V	−0.90 V	−0.93 V

of Na^+-ORR on Pt electrodes. In contrast, in the presence of cations larger than Cs^+, such as tetraalkylammonium (TAA^+) (ionic radius of 3.22 Å for tetramethylammonium (TMA^+)),[63,64] the ORR is a highly reversible (less negative $E_{1/2}$) one-electron process that involves the O_2/O_2^- couple,[65–67] according to:

$$O_2 + TAA^+ + e^- \rightarrow TAA^+\cdots O_2^- \quad (5)$$

Under steady-state conditions, Welford *et al.*[68] reported that the formation of O_2^- is limited by the diffusion of O_2 through the three-phase boundary O_2|electrode|electrolyte through the hanging meniscus in TAA^+-containing electrolytes with Au(111). These results suggest that the O_2^- species formation occurs exclusively *via* a solution-preferred mechanism limited by the diffusion of O_2, *i.e.*, with low surface specificity compared to Na^+.

In this paper, we suggest that the differences in the voltammetric response among alkali cations (Fig. 4) are due to a surface-mediated ORR for smaller cations, while larger cations prefer a solution-based mechanism dominated by the formation of O_2^-. When O_2 is reduced to O_2^-, larger cations stabilise O_2^- through ion-pair formation (ionic bonding), which allows a less negative $E_{1/2}$ for CsO_2 formation than for NaO_2.[11,69] The polarisability of the ionic bond decreases (the bond becomes more covalent in nature) for smaller alkali metals,[26] and therefore, such entities present increased peak separation in the voltammetric response and a more negative $E_{1/2}$. The fact that surface-adsorbed NaO_2 formed at the surface may also block metal active sites, thus inhibiting further ORR, may also play a part in the increase in ORR overpotential observed for Na^+ relative to Cs^+ in Fig. 4.

Differences in the peak current intensities among alkali metals are also observed in Fig. 4. The ratio of current between the O_2^- (I) and the O_2^{2-} (II) peaks is close to 1 for Na^+ and decreases for larger cations in the order $Na^+ > K^+ > Cs^+$.

This asymmetry could be related to the lifetime of the formed O_2^- complex. O_2^- in the presence of large cations could readily be solvated back into solution, which would reduce the number of species on the surface to undergo the second reduction to O_2^{2-} (II), which in turn results in lower currents and a more negative potential for the onset of the second reduction to O_2^{2-}. In addition, the separation of peaks I and II may also be affected. Upon the formation of strongly adsorbed NaO_2 at the surface of Pt(111), quantitative and rapid activation towards the formation of Na_2O_2 *via* Pt surface catalysis might be taking place. This would result in two effects in agreement with the data presented: (i) the intensity ratio of peak I to peak II being close to unity and (ii) the difference in potential between peaks I and II reflecting the extent of surface interaction of the adsorbed MO_2 complex (smallest peak separation for Na^+). Additionally, the intensity of the peak related to the oxidation of O_2^{2-} (III) also decays for larger cations ($Na^+ > K^+ > Cs^+$). In this sense, larger cations complexing with O_2^{2-} seem to have a more labile/dissociating nature compared to smaller cations, which would explain the lower intensity for the Cs_2O_2 electrooxidation (III) (upon formation, the complex decays or diffuses away prior to the positive-going sweep, leading to a lower intensity).

In order to further study the surface-dependence of the ORR among different alkali cations without the possibility of O_2 diffusion influencing the results, cyclic voltammetry in O_2-saturated DMSO containing Na^+, K^+, and Cs^+ was recorded,

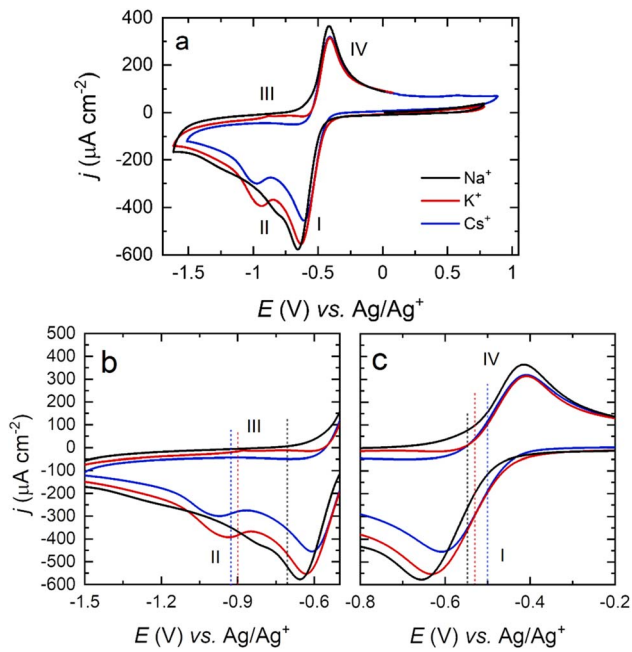

Fig. 5 (a) Cyclic voltammograms of a Pt(poly) electrode in an O_2-saturated DMSO solution containing 0.1 M $NaClO_4$ (black), $KClO_4$ (red) and $CsClO_4$ (blue), at 50 mV s^{-1} scan rate. Expanded view of the potential range corresponding to the formation of O_2^{2-} (b) and O_2^- (c). Dotted lines represent the $E_{1/2}$ of the ORR half reactions for Na^+ (black), K^+ (red) and Cs^+ (blue).

using a Pt polycrystalline disk electrode immersed in the electrolyte (no meniscus, Fig. 5).

The trends in the position of $E_{1/2}$ for the first and second reduction of O_2 as a function of metal cation are comparable both for Pt(111) and Pt(poly) electrodes (Table 2), with a small variation of *ca.* 30–40 mV associated with differences in surface structure.

While the current density ratio between the O_2^- (I) and O_2^{2-} (II) peaks is equivalent between Pt(111) and Pt(poly)using larger cations, *i.e.*, K^+ and Cs^+, the ratio in Na^+-containing DMSO differs, with a ratio close to 1 for Pt(111) and a ratio >1 for Pt(poly). Other previous studies have highlighted that both the surface and electrolyte have an impact on the Na^+-ORR mechanism.[30] In DMSO, Pt(110) and (111) facets support the formation of Na_2O_2 as the main reduction product on the surface, while on Pt(100) and polycrystalline surfaces, the formation of NaO_2 is less favoured and desorption and solvation is reported,[4,13] attributed to a more limited surface interaction of oxygen with electrode surfaces that do not contain {111} and {110} terrace sites.[24] This finding is consistent with the lower intensity of the redox peak associated with the formation of Na_2O_2 on Pt(poly) surfaces compared with Pt(111) and Pt(110). The NaO_2 surface complex in this case is less strongly interacting with the surface, so the activation of the second reduction step by the Pt(100) surface is much less marked, resulting in a lower intensity for peak II.

The difference in the relative current densities of the M^+–O_2^{2-} complex on the forward and reverse sweeps shows the same trend as for Pt(111) ($Cs^+ > K^+ > Na^+$), consistent with the dissociation/lability of the O_2^{2-} complex for larger cations, which suggests that Cs^+-ORR chemistry would be mostly dominated by solution-phase processes rather than being surface controlled.

While careful control of the crystal facet influences the reaction pathway, this is highly dependent on the cation of choice, as can be observed in Fig. 6. Shifts in the peak potential between the (111) and (100) facets for Na^+–O_2 OER/ORR are significant, whilst being negligible for Cs^+, differing by as much as $\pm$0.2 V for the first reduction and $\pm$0.3 V for the second reduction when Na^+ cations are present. These results again suggest that the surface structure has less effect on the ORR for larger alkali metals. The relative strength of adsorption for the peroxy- and superoxy-ion pairs would govern this behaviour, with those moieties formed by Cs^+ cations giving rise to the weakest surface interactions. This assertion is borne out during spectroscopic measurements, to be outlined below.

The change in nature for the ionic bond[26] between alkali cations and the O_2^- directly depends on the cation size, and increased polarisability of the ionic bond for larger alkali metals may affect the stability of superoxide complexes. To investigate the stability of O_2^- as a function of potential in the presence of a larger cation, *in situ* SHINERS spectra were collected with a Pt(111) electrode in 0.1 M $CsClO_4$/DMSO (Fig. 7a). The intensity of the band centred at 1160 cm^{-1}, corresponding to $\nu_{(O-O)}$ in O_2^-, can only be observed at -0.55 V, which correlates with the onset potential for the first reduction of O_2 to O_2^-. The band fades at more negative potentials, associated with the desorption of O_2^- from the surface of the electrode. These results differ from those previously reported for Na^+ in DMSO, where the band associated with $\nu_{(O-O)}$ can be observed even up to -1.0 V (at 1154 cm^{-1}).[24]

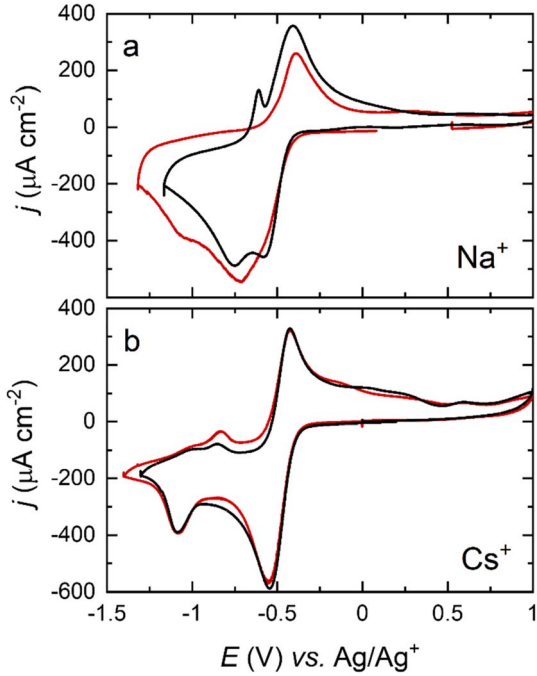

Fig. 6 Cyclic voltammograms of a Pt(111) (black) and a Pt(100) (red) electrode in an O_2-saturated DMSO solution containing (a) 0.1 M $NaClO_4$ and (b) 0.1 M $CsClO_4$. Scan rate: 50 mV s^{-1}.

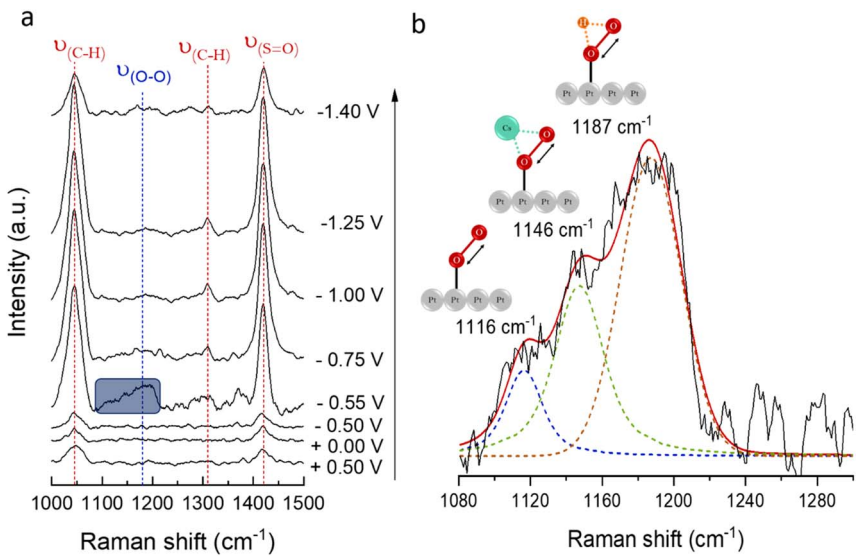

Fig. 7 (a) Potential-dependent *in situ* SHINERS spectra obtained from a Pt(111) electrode in a solution containing 0.1 M $CsClO_4$/DMSO, purged with Ar and, subsequently, saturated with O_2. (b) Voigt model fitting of $\nu_{(O-O)}$ at −0.55 V.

The deconvolution of the band centred at 1160 cm^{-1} is shown in Fig. 7b. The broad $\nu_{(O-O)}$ band has contributions from free O_2^- at 1116 cm^{-1}, CsO_2 at 1146 cm^{-1}, and HO_2 (most likely from minor traces of H_2O in the electrolyte) at 1187 cm^{-1}.[26,70]

The $\nu_{(O-O)}$ frequency shifts depend on the strength of the bond between the alkali cation and the O_2^-. Hence, the higher frequency observed for $\nu_{(O-O)}$ (NaO_2) at 1161 cm^{-1},[71,72] compared to $\nu_{(O-O)}$ (CsO_2) at 1146 cm^{-1},[13,24,26,73] may be ascribed to the ionic radii of the cations, *i.e.*, smaller cations display a substantial electrostatic force that strongly attracts the valence electrons from O_2^- and, therefore, present a stronger bonding interaction with the O_2^-. Additionally, while no free O_2^- has been detected in the presence of Na^+ (at equal alkali-metal concentrations),[24] spectroscopic evidence of the presence of free O_2^- (1116 cm^{-1}) in Cs^+-containing electrolytes (Fig. 7b) demonstrates the dissociation of O_2^- back into solution in the presence of larger cations.

Bands at 1040 and 1310 cm^{-1} correspond to the methyl-group rocking modes in DMSO and that at 1420 cm^{-1} to ν(S=O).[74–76] The bands associated with DMSO vibrations increase at −0.55 V, coinciding with the formation of O_2^- species at the electrode|electrolyte interface. Enhanced band intensity for DMSO at this potential may be due to the solvation of O_2^-, *i.e.*, $Cs^+(DMSO)_4(O_2^-)$. The further uptake of DMSO onto the Pt(111) surface following desorption of $Cs^+(DMSO)_4(O_2^-)$ species is also indicated by the significant increase in DMSO bands after this point. Increased DMSO band intensity in the potential range where ORR occurs has not been observed for Na^+,[24] probably due to DMSO less successfully competing for Pt sites with more strongly adsorbed NaO_2, *i.e.*, smaller cation–O_2^- complexes are more strongly adsorbed on the Pt(111) surface, while for larger cation–O_2^- complexes, adsorption is weaker, and they are readily desorbed back into solution. The lower intensity of the DMSO bands at −1.4 V could result from a potential-dependent reorientation of DMSO on the surface, similar to that reported for the reorientation of acetonitrile on roughened Au surfaces.[77]

Conclusions

The ORR and OER have been studied on Pt(111) and Pt(100) single crystals and on a polycrystalline Pt disk, using a non-aqueous solvent, dimethyl sulfoxide (DMSO), in the presence of alkali-metal perchlorate salts. Voltammetric results show that the cation size strongly affects the mechanism of the ORR in O_2-saturated DMSO-based electrolyte.

In contrast to Na^+, surface structure has been proved not to significantly influence the reaction pathway involving Cs^+ cations. This behaviour is ascribed to the relative surface adsorption strengths of superoxy and peroxy ion-pair complexes formed when utilising different cations. We conclude that because no changes were detected in the voltammetric profile of the ORR in the presence of Cs^+ cations using polycrystalline Pt, Pt(111) and Pt(100) electrodes, this supports a preferred solution-based mechanism with a lower impact of the surface structure compared to smaller cations, such as Na^+. Shifts in the $E_{1/2}$ and changes in the intensities of redox peaks I to IV as a function of cation size are also consistent with this finding. Moreover, the separation in potential between peaks I and II is suggested to be a marker for the extent of interaction between the electrode surface and MO_2. Because of this, it is speculated that activation of this

surface complex to facilitate the second electron transfer to form peroxy species will be promoted as cation size decrease, *i.e.*, the ORR pathway preference changes as the cation size increases, from O_2^{2-} formation in the case of Na^+ (and indeed Li^+) to O_2^- formation for larger cations, *i.e.*, K^+ and Cs^+.

To assess this proposal, the stability of the O_2^- complex adsorbed at the surface was studied with *in situ* Raman spectroscopy in Cs^+-containing electrolytes and results demonstrated the formation of CsO_2 in a limited potential range, commensurate with the first reduction peak, but this species readily desorbs into solution. The labile nature of the surface O_2^- bond is consistent with the lack of structural sensitivity in CV, suggesting a solution-based ORR/OER mechanism for larger cations. This may disfavour subsequent reduction to O_2^{2-} when using Cs^+ compared to Na^+ and this is made manifest by the relative magnitudes of peroxy- and superoxy-redox peaks highlighted above. Furthermore, *in situ* Raman spectroscopy indicates that the displacement of CsO_2 species may be ascribed to uptake of DMSO at the interface, interacting strongly with the surface and causing displacement of ion pairs at potentials where the ORR occurs. This study highlights the possibility of using large alkali-metal cations, such as Cs^+, in the electrolyte of Li and Na–O_2 cells to tailor the initial ORR pathway towards a one-electron transfer and thus, contributing to preventing the formation of surface-blocking peroxide intermediates.

Author contributions

All authors have contributed to writing, reviewing, and editing the final version of the manuscript. JFV contributed with investigation, methodology, data curation, conceptualisation, formal analysis, visualisation, and writing of the original draft. LJH contributed with funding acquisition, conceptualisation, formal analysis, supervision, resources, and project administration. GC contributed to investigation and methodology. GAA contributed to visualisation, supervision, formal analysis, and conceptualisation.

Conflicts of interest

All authors declare no conflict of interest.

Acknowledgements

JFV acknowledges PhD funding from the UKRI Engineering and Physical Sciences Research Council (EPSRC). LJH and GC acknowledge funding support from the UK Faraday Institution (EPSRC EP/S003053/1) through the Degradation Project (grant numbers FIRG001 and FIRG024). We acknowledge discussions with Dr Tom Galloway.

References

1 S. A. Freunberger, Y. Chen, N. E. Drewett, L. J. Hardwick, F. Bardé and P. G. Bruce, The lithium–oxygen battery with ether-based electrolytes, *Angew. Chem., Int. Ed.*, 2011, **50**, 8609–8613.

2 D. Sharon, D. Hirshberg, M. Afri, A. A. Frimer, M. Noked and D. Aurbach, Aprotic Metal–Oxygen Batteries: Recent Findings and Insights, *J. Solid State Electrochem.*, 2017, **21**, 1861–1878.
3 T. A. Galloway, G. Attard and L. J. Hardwick, An Electrochemical Investigation of Oxygen Adsorption on Pt Single Crystal Electrodes in a Non-Aqueous Li+ Electrolyte, *Electrochem. Commun.*, 2020, **119**, 106814.
4 T. A. Galloway, L. Cabo-Fernandez, I. M. Aldous, F. Braga and L. J. Hardwick, Shell Isolated Nanoparticles for Enhanced Raman Spectroscopy Studies in Lithium–Oxygen Cells, *Faraday Discuss.*, 2017, **205**, 469–490.
5 Y. Chen, S. A. Freunberger, Z. Peng, O. Fontaine and P. G. Bruce, Charging a Li–O_2 Battery Using a Redox Mediator, *Nat. Chem.*, 2013, **5**, 489–494.
6 P. Reinsberg, A. Weiß, P. P. Bawol and H. Baltruschat, Electrochemical Reaction Order of the Oxygen Reduction Reaction in Li^+-Containing DMSO, *J. Phys. Chem. C*, 2017, **121**, 7677–7688.
7 A. I. Belova, D. G. Kwabi, L. V. Yashina, Y. Shao-Horn and D. M. Itkis, Mechanism of Oxygen Reduction in Aprotic Li-air Batteries: The Role of Carbon Electrode Surface Structure, *J. Phys. Chem. C*, 2017, **121**, 1569–1577.
8 W. Wang and Y. C. Lu, The Potassium–Air Battery: Far from a Practical Reality?, *Acc. Mater. Res.*, 2021, **2**, 515–525.
9 P. Hartmann, C. L. Bender, M. Vračar, A. K. Dürr, A. Garsuch, J. Janek and P. Adelhelm, A Rechargeable Room-Temperature Sodium Superoxide (NaO_2) Battery, *Nat. Mater.*, 2013, **12**, 228–232.
10 X. Ren and Y. Wu, A Low-Overpotential Potassium–Oxygen Battery Based on Potassium Superoxide, *J. Am. Chem. Soc.*, 2013, **135**, 2923–2926.
11 C. J. Bondue, P. P. Bawol, A. A. Abd-El-Latif, P. Reinsberg and H. Baltruschat, Gaining Control over the Mechanism of Oxygen Reduction in Organic Electrolytes: The Effect of Solvent Properties, *J. Phys. Chem. C*, 2017, **121**, 8864–8872.
12 C. J. Bondue, P. Reinsberg, A. A. Abd-El-Latif and H. Baltruschat, Oxygen Reduction and Oxygen Evolution in DMSO Based Electrolytes: The Role of the Electrocatalyst, *Phys. Chem. Chem. Phys.*, 2015, **17**, 25593–25606.
13 I. M. Aldous and L. J. Hardwick, Solvent-Mediated Control of the Electrochemical Discharge Products of Non-Aqueous Sodium–Oxygen Electrochemistry, *Angew. Chem., Int. Ed.*, 2016, **55**, 8254–8257.
14 P. M. Radjenovic and L. J. Hardwick, Time-resolved SERS study of the oxygen reduction reaction in ionic liquid electrolytes for non-aqueous lithium-oxygen cells, *Faraday Discuss.*, 2018, **206**, 379–392.
15 L. Johnson, C. Li, Z. Liu, Y. Chen, S. Freunberger, P. Ashok, B. Praveen, K. Dholakia, J. Tarascon and P. Bruce, The Role of LiO_2 Solubility in O_2 Reduction in Aprotic Solvents and its Consequences for Li–O_2 Batteries, *Nat. Chem.*, 2014, **6**, 1091–1099.
16 N. Mozhzhukhina, L. P. Méndez De Leo and E. J. Calvo, Infrared Spectroscopy Studies on Stability of Dimethyl Sulfoxide for Application in a Li–Air Battery, *J. Phys. Chem. C*, 2013, **117**, 18375–18380.
17 M. A. Schroeder, N. Kumar, A. J. Pearse, C. Liu, S. B. Lee, G. W. Rubloff, K. Leung and M. Noked, DMSO-Li_2O_2 Interface in the Rechargeable Li–O_2 Battery Cathode: Theoretical and Experimental Perspectives on Stability, *ACS Appl. Mater. Interfaces*, 2015, **7**, 11402–11411.

18 V. Gutmann, *The Donor–Acceptor Approach to Molecular Interactions*, Springer, US, 1978.
19 V. Gutmann, Solvent Effects on the Reactivities of Organometallic Compounds, *Coord. Chem. Rev.*, 1976, **18**, 225–255.
20 A. D. Goolsby and D. T. Sawyer, The Electrochemical Reduction of Superoxide Ion and Oxidation of Hydroxide Ion in Dimethyl Sulfoxided, *Anal. Chem.*, 1968, **40**, 83–86.
21 T. Kumeda, H. Tajiri, O. Sakata, N. Hoshi and M. Nakamura, Effect of hydrophobic cations on the oxygen reduction reaction on single-crystal platinum electrodes, *Nat. Commun.*, 2018, **9**, 4378.
22 D. Strmcnik, K. Kodama, D. Van Der Vliet, J. Greeley, V. R. Stamenkovic and N. M. Marković, The Role of Non-Covalent Interactions in Electrocatalytic Fuel-Cell Reactions on Platinum, *Nat. Chem.*, 2009, **1**, 466–472.
23 P. H. Reinsberg, A. Koellisch and H. Baltruschat, On the Importance of Ion Pair Formation and the Effect of Water in Potassium–Oxygen Batteries, *Electrochim. Acta*, 2019, **313**, 223–234.
24 T. A. Galloway, J.-C. Dong, J.-F. Li, G. Attard and L. J. Hardwick, Oxygen Reactions on Pt{hkl} in a Non-Aqueous Na^+ Electrolyte: Site Selective Stabilisation of a Sodium Peroxy Species, *Chem. Sci.*, 2019, **10**, 2956–2964.
25 S. Ma, W. C. McKee, J. Wang, L. Guo, M. Jansen, Y. Xu and Z. Peng, Mechanistic Origin of Low Polarization in Aprotic Na–O_2 Batteries, *Phys. Chem. Chem. Phys.*, 2017, **19**, 12375–12383.
26 P. M. Radjenovic and L. J. Hardwick, Evaluating Chemical Bonding in Dioxides for the Development of Metal–Oxygen Batteries: Vibrational Spectroscopic Trends of Dioxygenyls, Dioxygen, Superoxides and Peroxides, *Phys. Chem. Chem. Phys.*, 2019, **21**, 1552–1563.
27 P. G. Bruce, L. J. Hardwick and K. M. Abraham, Lithium–Air and Lithium–Sulfur Batteries, *MRS Bull.*, 2011, **36**, 506–512.
28 T. Zhang, Z. Xu, Y. Guo, C. Liang, J. Wang and J. Yang, Building High Performance Silicon–Oxygen and Silicon–Sulfur Battery by In-Situ Lithiation of Fibrous Si/C Anode, *J. Alloys Compd.*, 2019, **806**, 335–342.
29 S. K. Das, S. Lau and L. A. Archer, Sodium–Oxygen Batteries: A New Class of Metal–Air Batteries, *J. Mater. Chem. A*, 2014, **2**, 12623–12629.
30 C. L. Bender, D. Schröder, R. Pinedo, P. Adelhelm and J. Janek, One- or Two-Electron Transfer? The Ambiguous Nature of the Discharge Products in Sodium-Oxygen Batteries, *Angew. Chem., Int. Ed.*, 2016, **55**, 4640–4649.
31 H. Yadegari, Q. Sun and X. Sun, Sodium–Oxygen Batteries: A Comparative Review from Chemical and Electrochemical Fundamentals to Future Perspective, *Adv. Mater.*, 2016, **28**, 7065–7093.
32 P. H. Reinsberg, A. Koellisch, P. P. Bawol and H. Baltruschat, K–O_2 Electrochemistry: Achieving Highly Reversible Peroxide Formation, *Phys. Chem. Chem. Phys.*, 2019, **21**, 4286–4294.
33 L. Xue, Y. Li, H. Gao, W. Zhou, X. Lü, W. Kaveevivitchai, A. Manthiram and J. B. Goodenough, Low-Cost High-Energy Potassium Cathode, *J. Am. Chem. Soc.*, 2017, **139**, 2164–2167.
34 N. Xiao, X. Ren, W. D. McCulloch, G. Gourdin and Y. Wu, Potassium Superoxide: A Unique Alternative for Metal–Air Batteries, *Acc. Chem. Res.*, 2018, **51**, 2335–2343.

35 P. K. Shen and Z. Zhao, Mechanism of Oxygen Reduction Reaction, in *Electrochemical Oxygen Reduction: Fundamental and Applications*, ed. P. K. Shen, Springer, 2021, pp. 11–22.
36 N. M. Marković, T. J. Schmidt, V. Stamenković and P. N. Ross, Oxygen Reduction Reaction on Pt and Pt Bimetallic Surfaces: A Selective Review, *Fuel Cells*, 2001, **1**, 105–116.
37 A. M. Gómez-Marín and J. M. Feliu, New insights into the oxygen reduction reaction mechanism on Pt (111): a detailed electrochemical study, *ChemSusChem*, 2013, **6**, 1091–1100.
38 J. Zhang, Y. Mo, M. B. Vukmirovic, R. Klie, K. Sasaki and R. R. Adzic, Platinum Monolayer Electrocatalysts for O_2 Reduction: Pt Monolayer on Pd(111) and on Carbon-Supported Pd Nanoparticles, *J. Phys. Chem. B*, 2004, **108**, 10955–10964.
39 X. Zhang, H. Li, J. Yang, Y. Lei, C. Wang, J. Wang, Y. Tang and Z. Mao, Recent Advances in Pt-based Electrocatalysts for PEMFCs, *RSC Adv.*, 2021, **11**, 13316–13328.
40 C. Song and J. Zhang, Electrocatalytic Oxygen Reduction Reaction, in *PEM Fuel Cell Electrocatalysts and Catalyst Layers: Fundamentals and Applications*, 2008.
41 A. Haryanto and C. W. Lee, Shell Isolated Nanoparticle Enhanced Raman Spectroscopy for Mechanistic Investigation of Electrochemical Reactions, *Nano Converg.*, 2022, **9**, 9.
42 Y.-J. Zhang, H. Ze, P.-P. Fang, Y.-F. Huang, A. Kudelski, J. Fernández-Vidal, L. J. Hardwick, J. Lipkowski, Z.-Q. Tian and J.-F. Li, Shell-isolated nanoparticleenhanced Raman spectroscopy, *Nat. Rev. Methods Primers*, 2023, 1–22.
43 J.-C. C. Dong, X.-G. G. Zhang, V. Briega-Martos, X. Jin, J. Yang, S. Chen, Z.-L. L. Yang, D.-Y. Y. Wu, J. M. Feliu, C. T. Williams, Z. Q. Tian and J. F. Li, In situ Raman spectroscopic evidence for oxygen reduction reaction intermediates at platinum single-crystal surfaces, *Nat. Energy*, 2019, **4**, 60–67.
44 Y.-F. Huang, P. J. Kooyman and M. T. M. Koper, Intermediate Stages of Electrochemical Oxidation of Single-Crystalline Platinum Revealed by In Situ Raman Spectroscopy, *Nat. Commun.*, 2016, **7**, 12440.
45 R. Rizo, J. Fernández-Vidal, L. J. Hardwick, G. A. Attard, F. J. Vidal-Iglesias, V. Climent, E. Herrero and J. M. Feliu, Investigating the Presence of Adsorbed Species on Pt Steps at Low Potentials, *Nat. Commun.*, 2022, **13**, 2550.
46 J. Clavilier, R. Faure, G. Guinet and R. Durand, Preparation of monocrystalline Pt microelectrodes and electrochemical study of the plane surfaces cut in the direction of the {111} and {110} planes, *J. Electroanal. Chem.*, 1980, **107**, 205–209.
47 A. M. Bittner, J. Wintterlin, B. Beran and G. Ertl, Bromine adsorption on Pt(111), (100), and (110)-an STM study in air and in electrolyte, *Surf. Sci.*, 1995, **335**, 291–299.
48 H. Oguz, N. Yokoi and S. Kinoshita, The Height and Radius of the Tear Meniscus and Methods for Examining These Parameters, *Cornea*, 2000, **19**, 497–500.
49 K. Momma and F. Izumi, VESTA 3 for Three-Dimensional Visualization of Crystal, Voltammetric and Morphology Data, *J. Appl. Crystallogr.*, 2011, **44**, 1272–1276.
50 C. G. Zoski, *Handbook of Electrochemistry*, Elsevier, 2007.
51 J. Turkevich, Colloidal gold. Part I, *Gold Bull.*, 1985, **18**, 86–91.

52 J. Turkevich, P. C. Stevenson and J. Hiller, Synthesis of Gold Nanoparticles Turkevich method, *Discuss. Faraday Soc.*, 1951, **11**, 55–75.
53 G. Frens, Controlled Nucleation for the Regulation of the Particle Size in Monodisperse Gold Suspensions, *Nat. Phys. Sci.*, 1973, **241**, 20–22.
54 L. M. Liz-Marzán, M. Giersig and P. Mulvaney, Synthesis of Nanosized Gold–Silica Core–Shell Particles, *Langmuir*, 1996, **12**, 4329–4335.
55 C. Hanske, M. N. Sanz-Ortiz and L. M. Liz-Marzán, Silica-Coated Plasmonic Metal Nanoparticles in Action, *Adv. Mater.*, 2018, **30**, 1707003.
56 J. F. Li, Y. F. Huang, Y. Ding, Z. L. Yang, S. B. Li, X. S. Zhou, F. R. Fan, W. Zhang, Z. Y. Zhou, D. Y. Wu, B. Ren, Z. L. Wang and Z. Q. Tian, Shell-Isolated Nanoparticle-Enhanced Raman Spectroscopy, *Nature*, 2010, **464**, 392–395.
57 C. O. Laoire, S. Mukerjee, K. M. Abraham, E. J. Plichta and M. A. Hendrickson, Elucidating the Mechanism of Oxygen Reduction for Lithium–Air Battery Applications, *J. Phys. Chem. C*, 2009, **113**, 20127–20134.
58 K. M. Abraham and Z. A. Jiang, Polymer Electrolyte-Based Rechargeable Lithium/Oxygen Battery, *J. Electrochem. Soc.*, 1996, **143**, 1–5.
59 K. M. Abraham, Z. Jiang and B. Carroll, Highly Conductive PEO-like Polymer Electrolytes, *Chem. Mater.*, 1997, **9**, 1978–1988.
60 H. S. Choe, B. G. Carroll, D. M. Pasquariello and K. M. Abraham, Characterization of Some Polyacrylonitrile-Based Electrolytes, *Chem. Mater.*, 1997, **9**, 369–379.
61 S. S. Zhang, D. Foster and J. Read, The Effect of Quaternary Ammonium on Discharge Characteristic of a Non-Aqueous Electrolyte Li/O_2 Battery, *Electrochim. Acta*, 2011, **56**, 1283–1287.
62 R. D. Shannon, Revised Effective Ionic Radii and Systematic Studies of Interatomic Distances in Halides and Chalcogenides, *Acta Crystallogr. A*, 1976, **32**, 751–767.
63 J. Palomo and P. N. Pintauro, Competitive Absorption of Quaternary Ammonium and Alkali Metal Cations into a Nafion Cation-Exchange Membrane, *J. Membr. Sci.*, 2003, **215**, 103–114.
64 D. H. Aue, H. M. Webb and M. T. Bowers, A Thermodynamic Analysis of Solvation Effects on the Basicities of Alkylamines. An Electrostatic Analysis of Substituent Effects, *J. Am. Chem. Soc.*, 1976, **98**, 318–329.
65 C. O. Laoire, S. Mukerjee, K. M. Abraham, E. J. Plichta and M. A. Hendrickson, Influence of Nonaqueous Solvents on the Electrochemistry of Oxygen in the Rechargeable Lithium–Air Battery, *J. Phys. Chem. C*, 2010, **114**, 9178–9186.
66 Y.-T. Lu, A. R. Neale, C.-C. Hu and L. J. Hardwick, Trapped Interfacial Redox Introduces Reversibility in the Oxygen Reduction Reaction in a Non-Aqueous Ca^{2+} Electrolyte, *Chem. Sci.*, 2021, **12**, 8909–8919.
67 C. J. Bondue, A. A. Abd-El-Latif, P. Hegemann and H. Baltruschat, Quantitative Study for Oxygen Reduction and Evolution in Aprotic Organic Electrolytes at Gas Diffusion Electrodes by DEMS, *J. Electrochem. Soc.*, 2015, **162**, A479–A487.
68 P. J. Welford, B. A. Brookes, V. Climent and R. G. Compton, The hanging meniscus contact: geometry induced diffusional overpotential. The reduction of oxygen in dimethylsulphoxide at Au(111), *J. Electroanal. Chem.*, 2001, **513**, 8–15.
69 I. I. Vol'nov, *Peroxides, Superoxides, and Ozonides of Alkali and Alkaline Earth Metals*, Springer, US, 1966.

70 X. Li and A. A. Gewirth, Oxygen Electroreduction through a Superoxide Intermediate on Bi-Modified Au Surfaces, *J. Am. Chem. Soc.*, 2005, **127**, 5252–5260.

71 J. B. Bates and M. H. Brooker, Determination of Longitudinal Optical Mode Frequencies by Polarized Specular Reflectance Infrared Spectroscopy, *J. Phys. Chem. Solids*, 1971, **32**, 2403–2407.

72 J. B. Bates, M. H. Brooker, A. S. Quist and G. E. Boyd, Raman Spectra of Molten Alkali Metal Carbonates, *J. Phys. Chem.*, 1972, **76**, 1565–1571.

73 J. B. Bates, M. H. Brooker and G. E. Boyd, Raman Spectra of O^{-2} and O^{-3} Ions in Alkali-Metal Superoxides and Ozonides, *Chem. Phys. Lett.*, 1972, **16**, 391–395.

74 V. M. Wallace, N. R. Dhumal, F. M. Zehentbauer, H. J. Kim and J. Kiefer, Revisiting the Aqueous Solutions of Dimethyl Sulfoxide by Spectroscopy in the Mid- and Near-Infrared: Experiments and Car-Parrinello Simulations, *J. Phys. Chem. B*, 2015, **119**, 14780.

75 Q. Yu and S. Ye, In Situ Study of Oxygen Reduction in Dimethyl Sulfoxide (DMSO) Solution: A Fundamental Study for Development of the Lithium–Oxygen Battery, *J. Phys. Chem. C*, 2015, **119**, 12236–12250.

76 C. Xu, A. Ge, K. Kannari, B. Peng, M. Xue, B. Ding, K. Inoue, X. Zhang and S. Ye, The Decisive Role of Li_2O_2 Desorption for Oxygen Reduction Reaction in Li–O_2 Batteries, *ACS Energy Lett.*, 2023, **8**, 1289–1299.

77 I. M. Aldous and L. J. Hardwick, Influence of tetraalkylammonium cation chain length on gold and glassy carbon electrode interfaces for alkali metal–oxygen batteries, *J. Phys. Chem. Lett.*, 2014, **5**, 3924–3930.

